remote sensing

MDPI

Article

A Sentinel-1 Based Hybrid Interferometric Approach to Complement EGMS for Landslides Identification

Matteo Mantovani [1], Federica Ceccotto [1,*], Angelo Ballaera [1], Emilia Bertorelle [1,2], Giulia Bossi [1], Gianluca Marcato [1] and Alessandro Pasuto [1]

[1] National Research Council, Research Institute for Geo-Hydrological Protection (CNR-IRPI), Corso Stati Uniti 4, 35127 Padova, Italy; matteo.mantovani@cnr.it (M.M.); angelo.ballaera@cnr.it (A.B.); brtmle@unife.it or emiliabertorelle@cnr.it (E.B.); giulia.bossi@cnr.it (G.B.); gianluca.marcato@cnr.it (G.M.); alessandro.pasuto@cnr.it (A.P.)

[2] Dipartimento di Fisica e Scienze della Terra, Università degli Studi di Ferrara, Via Giuseppe Saragat 1, 44122 Ferrara, Italy

* Correspondence: federica.ceccotto@cnr.it

Highlights

What are the main findings?

- HIA maximizes the number of coherent targets on the ground.
- HIA complements EGMS products.

What are the implications of the main findings?

- HIA offers an enhanced capacity in landslide detection.
- HIA contributes to landslide hazard assessment.

Abstract

This study introduces a Hybrid Interferometric Approach (HIA) tailored for the detection, mapping, and measurement of landslides using Sentinel-1 satellite data. The HIA is specifically designed to identify ground displacements that exceed the detection thresholds of the European Ground Motion Service (EGMS), offering an enhanced capacity for monitoring faster-moving landslides. The methodology integrates multi-baseline interferometric analysis, utilizing backscattered signals from both point-like and distributed radar targets at full spatial resolution. The approach utilizes ten interferometric datasets acquired between 2017 and 2021 from both ascending and descending orbits. Each annual dataset is restricted to a six-month observation window to reduce temporal decorrelation effects. The HIA was implemented in a landslide-prone sector of the Dolomites, a UNESCO World Heritage Site located in the Eastern Italian Alps. Comparative evaluation against EGMS ground motion products demonstrates that the HIA significantly broadens the range of detectable slope instabilities, thus providing a valuable supplement to existing ground motion monitoring services and contributing meaningfully to landslide hazard assessment and risk reduction efforts.

Keywords: EGMS; Sentinel-1; InSAR; landslides; Dolomites

check for updates

Academic Editor: Michele Saroli

Received: 13 October 2025
Revised: 14 November 2025
Accepted: 24 November 2025
Published: 27 November 2025

Citation: Mantovani, M.; Ceccotto, F.; Ballaera, A.; Bertorelle, E.; Bossi, G.; Marcato, G.; Pasuto, A. A Sentinel-1 Based Hybrid Interferometric Approach to Complement EGMS for Landslides Identification. *Remote Sens.* **2025**, *17*, 3849. https://doi.org/10.3390/rs17233849

Copyright: © 2025 by the authors. Licensee MDPI, Basel, Switzerland. This article is an open access article distributed under the terms and conditions of the Creative Commons Attribution (CC BY) license (https://creativecommons.org/licenses/by/4.0/).

1. Introduction

The Earth's surface is continuously deforming due to both natural processes, such as tectonic activity and volcanism, and human activities, including groundwater extraction

and mining. These ground movements can significantly impact infrastructures, ecosystems, and human safety, driving the need for reliable and comprehensive monitoring solutions.

Among the most advanced Earth observation techniques, imaging radar remote sensing has rapidly evolved into a dynamic and fast-advancing field in geoscience [1–3]. This progress is reflected in the growing number of space missions leveraging the capabilities of satellites equipped with Synthetic Aperture Radar (SAR) [4–11], which has fostered the development of numerous data processing techniques and analysis tools [12–14]. These approaches, collectively known as Advanced DInSAR (A-DInSAR) or Time Series Radar Interferometry (TS-InSAR), represent different implementations of two principal methodologies: Persistent Scatterer Interferometry (PSI) [15], which focuses on identifying stable, point-like natural targets within stacks of interferograms, and Small Baseline Subsets (SBAS) [16], which exploits the optimal spatial and temporal relationships among radar acquisitions.

In 2016, a group of 75 interferometric SAR (InSAR) data experts from across the European Union (EU) collaborated to develop the conceptual foundation for the implementation of the European Ground Motion Service (EGMS) [17]. Nowadays, the EGMS represents a pioneering application of InSAR technology on a continental scale providing free and accessible millimeter-precision measurements of ground deformation across Europe's Copernicus Program Participating States, offering a crucial tool for the scientific community, urban planners, and public authorities to assess natural hazards, impacts of climate change, and infrastructure structural integrity. EGMS is based on the full resolution processing of the images acquired by the Sentinel-1 mission and integrates both persistent scatterers (PS) and distributed scatterers (DS) in InSAR methodologies, further refined through a high-quality Global Navigation Satellite System (GNSS) model for geodetic referencing. This approach ensures accurate and consistent ground motion measurements, facilitating seamless cross-border analysis and interpretation. To maximize usability, EGMS provides a suite of visualization, analysis, and data-download tools, fostering user engagement and best-practice applications. The first baseline product, covering data from 2015–2020, was released in early 2022, with annual updates ensuring the continuous monitoring of ground motion trends across Europe [18].

Landslides are recognized as one of the most pervasive natural hazards, yet their full impact, both economic and societal, often remains underreported [19]. According to a 2012 Scientific and Policy Report by the Joint Research Centre of the European Commission [20], more than 633,000 landslides have been documented in national databases across the EU. However, this figure is estimated to represent less than half of the actual occurrences.

Despite the capabilities of InSAR, landslide-induced ground deformation presents a unique challenge for detection and monitoring [21]. EGMS itself is subject to these limitations, which stem from various factors including slope geometry, vegetation cover, displacement velocity, and the specific kinematics of the landslide process [22].

This study introduces a Hybrid Interferometric Approach (HIA) based on a Sentinel-1 dataset and tailored to map, detect, and measure landslide displacements with rates higher than those typically detectable by the EGMS.

The proposed methodology builds upon established interferometric techniques and algorithms, performing a multi-baseline interferometric analysis that utilizes backscattered signals from both point-like and distributed radar targets at full resolution. The analysis is based on ten datasets acquired between 2017 and 2021 from both ascending and descending orbits but is limited to six months per year, from the beginning of May to late October, to reduce temporal decorrelation and minimize the influence of snow cover. The relatively short observation window represents the distinctive aspect of the HIA approach, which, combined with the 6-day revisit time of the Sentinel-1 mission, enables the generation

of a sufficient number of interferograms to perform regression analyses, allowing the interferometric phase to be interpreted in terms of surface displacements. The study focuses on a region within the Dolomites UNESCO World Heritage site in the Eastern Italian Alps, affected by a large number of landslides.

The obtained results are compared with the products provided by the EGMS, the data from the Italian Landslide Inventory (IFFI Project), and information gathered from the bibliographic review of previously published studies conducted in the test area.

By expanding the range of detectable landslides, the HIA enhances existing EGMS products and provides valuable contributions to landslide risk assessment and mitigation, ensuring improved coverage of critical ground measurement points. Furthermore, the HIA approach can be applied to other geographic settings—not only mountainous regions but also areas with sparse vegetation—to investigate ground deformations caused by natural processes or human activities. Overall, the ability to improve ground deformation detection carries significant practical relevance for infrastructure protection, land management optimization, and supporting climate change adaptation strategies.

2. Test Site

The study area encompasses a portion of the Alta Badia Valley and the upper Cordevole River basin, straddling the provinces of Bolzano and Belluno in the Eastern Italian Alps (Figure 1). Covering approximately 236 km^2, the region exhibits a wide altitudinal range, from around 1000 m up to over 3100 m above sea level.

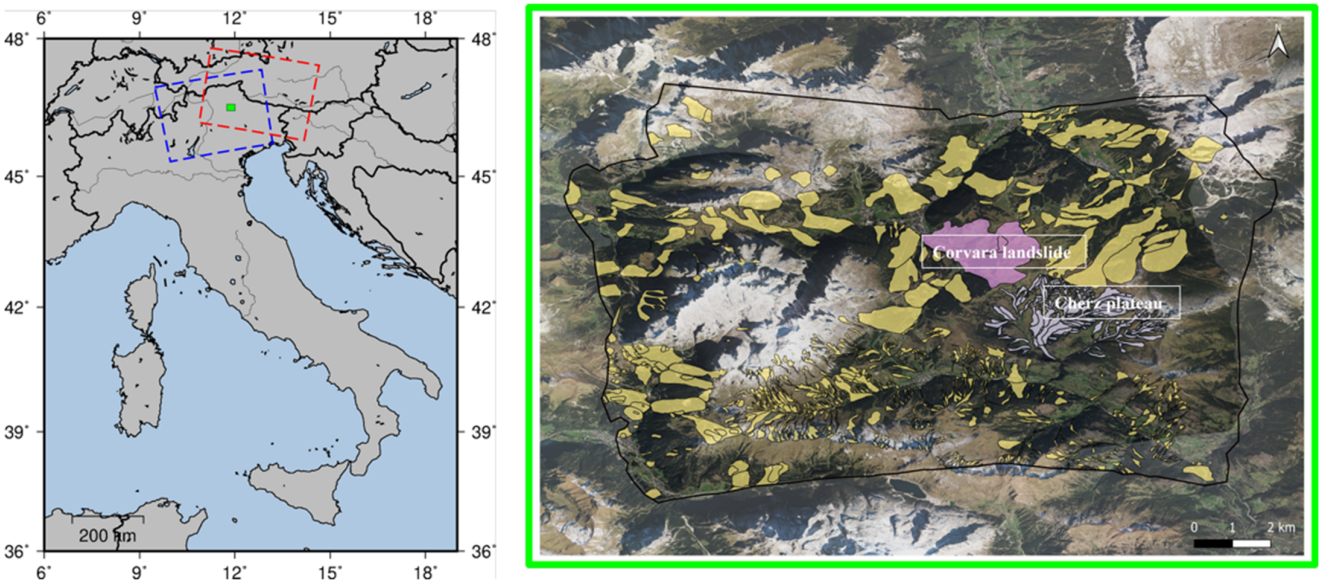


Figure 1. On the left, map showing the location of the area of interest, outlined by the green rectangle. Dashed lines indicate the coverage swaths of Sentinel-1 acquisitions: track ascending 117 in blue and track descending 95 in red. On the right optical satellite image (Map data ©2022 Bing Satellite) showing the test site outlined in black. Landslides within the area of interest are shown in light yellow; the Corvara landslide is highlighted in fuchsia, and the Cherz Plateau in light purple.

The area's long and complex geological and geomorphological evolution has given rise to striking landscapes, characterized by towering vertical dolomite cliffs emerging from gentler slopes composed of darker terrains. These lower slopes host forests, alpine pastures, scattered settlements, and a range of tourism-related infrastructure. Signs of slope instability are evident both on the steep dolomite rock faces and on the less steep marly and clay-rich terrains. In particular, rock falls, topples, and rock slides are prevalent in the heavily fractured dolomites, while earth flows and earth slides primarily affect the

underlying softer materials. These finer-grained terrains are also subject to solifluction, leading to characteristic surface features such as lobes, ripples, and extensional cracks.

Frequent intense rainfall events in the region promote debris flows, which mobilize loose debris from scree slopes and talus cones. Shallow ground movements and surface deformations are also common in plastic materials, particularly in areas where the topography alternates between concave and convex forms, conditions that enhance soil saturation and promote slow movement. Based on data from the Italian Landslide Inventory (IFFI Project) [23], 910 landslides have been identified within the study area, affecting approximately 23.7% of the total surface. Earth slides and earth flows are the most prevalent types. These landslides often exhibit complex or composite morphologies [24]. Within the broader study area, two sites were examined in detail: the Cherz plateau and the Corvara in Badia landslide.

The Cherz plateau is underlain by alternating layers of marls and sandstones, a lithological configuration that, combined with intense precipitations, contributes to the prevalence of landslides, primarily rotational slides and earth flows. A study by [25] identified nearly 200 landslides on the plateau, exhibiting a wide range of displacement velocities and morphological characteristics. GNSS monitoring carried out between November 2004 and July 2006 revealed that most of the 30 installed benchmarks registered movement rates between 0.20 and 1.20 m/year. To the best of our knowledge, the Cherz Plateau has received limited attention from the scientific community, and no specific space-borne SAR investigations have been reported for this area.

The Corvara in Badia landslide is the most significant mass movement within the study area, both in terms of scale and hazard potential, as extensively documented in scientific literature. It is classified as a slump-earth flow moving westward and involves approximately 120 to 150 million cubic meters of clay-rich material. The landslide covers an area of around 3 km^2 and has an estimated thickness ranging from 40 to 45 m [26]. Continuous monitoring of the slope has been in place since 1997 through various field-based instruments for hazard assessment. Between 2000 and 2002, data collected using GNSS, inclinometers, downhole extensometers, and TDR cables revealed displacement rates ranging from 0.10 to 1.00 m/year [27].

In more recent years, the Corvara landslide has also been investigated using satellite-based radar interferometry. Ref. [28] employed Multi-Temporal Interferometry using Permanent Scatterers, combined with 16 artificial Corner Reflectors, to assess surface displacements using X-band COSMO-SkyMed imagery. Ref. [29] conducted long-term monitoring by integrating data from Envisat, Radarsat-1, and COSMO-SkyMed missions. More recently, Ref. [30] applied the Small Baseline Subset (SBAS) technique to a set of Sentinel-1 acquisitions, further enhancing the understanding of slope dynamics in this area.

The stunning landscape surrounding the Cherz Plateau and the town of Corvara makes this area a highly popular destination for both winter and summer tourism. Its terrain is interwoven with renowned hiking trails that connect mountain refuges, scenic viewpoints, and various tourist accommodations, drawing visitors year-round. However, the active movements of the landslides pose a persistent challenge: ongoing ground displacements frequently damage key infrastructure, including ski facilities, a golf course, and the national road that serves as a vital access route. The lower end of the Corvara landslide reaches the town, grazing some buildings.

These instabilities represent not only a significant maintenance burden but also a serious safety concern, highlighting the importance of continuous monitoring and effective risk mitigation in such a valuable and heavily frequented area.

3. Materials and Methods

The HIA embraces existing interferometric techniques and algorithms to gain further insight into landslide-induced displacements, beyond the information extracted from the products offered by the EGMS. In particular, the HIA is tailored with the objectives to increase the spatial sampling of measurement points on the ground (enhancing spatial coverage) and to detect, map, and measure potential faster (in the order of 10^{-1} m/year) in non-uniform ground displacements that may not be identifiable in the EGMS data.

The HIA utilizes both Sentinel-1A and -1B VV-polarized datasets acquired from 2017 until 2021 when the two satellites operated simultaneously, with an evenly six-day repeat orbit cycle. For each year separately, 30 images both on ascending and descending orbits, covering a six-month period were analyzed. To minimize the effect of snow coverage, the images were chosen from the beginning of May to late October. Due to missing acquisitions in the ascending path, the processing for the years 2019 and 2021 followed a slightly different procedure (Table 1).

Table 1. Specifications of the dataset used in this study and key details of the processing procedure.

Path	Year	No. Images	First–Last Image Date	Missing Images Date	Max. Temporal Baseline (days)	No. Interferograms
Ascending 117	2017	30	6 May–27 October		12	57
	2018	30	7 May–28 October		12	57
	2019	30	2 May–29 October	23 September	12	55
	2020	30	8 May–29 October		12	57
	2021	27	9 May–30 October	8 June–19 August–25 August	18	67
Descending 95	2017	30	5 May–26 October		12	57
	2018	30	6 May–27 October		12	57
	2019	30	7 May–28 October		12	57
	2020	30	7 May–28 October		12	57
	2021	30	8 May–29 October		12	57

The interferometric processing chain can be visualized in the flowchart of Figure 2. The processing strategy builds upon the methodology proposed in [31] and is composed of two main stages.

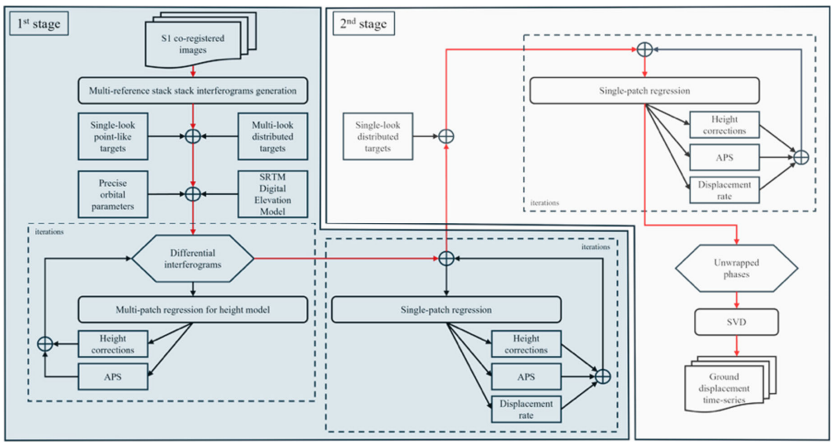


Figure 2. Flowchart of HIA processing strategy.

Initially, a multi-reference interferometric stack was generated, comprising interferometric pairs formed with multiple reference scenes. This setup ensures an overabundance of observations. The pairs were deliberately selected with short temporal baselines—no longer than 12 days—to guarantee double redundancy. With a total of 30 images, this configuration yielded 57 interferograms, as expressed by the following relation:

$$\sqrt{I = (N, S) = \sum_{i=1}^{S} (N - i)}, \quad (1)$$

where N stands for the quantity of SAR images (30), S is the maximum number of consecutive images to pair to create the interferograms (2), and I is the amount of generated interferograms (57).

The first stage employs both single-look and multi-look phase targets. Multi-looking is used to reduce phase noise in the differential interferograms, potentially enhancing the phase quality compared to single-pixel targets, and thereby increasing the spatial coverage. Specifically, a multi-looking factor of 27 in the range direction and 3 in the azimuth direction was applied to achieve this goal and maintain comparable spacing between the range and azimuth dimensions.

Multi-look phase targets are identified by averaging the spatial coherence across the entire image stack and applying a low-threshold mask to exclude areas affected by layover, shadow, or surfaces covered by water, snow, and high vegetation. Single-look targets are selected based on their low spectral phase diversity, a criteria suitable for smaller datasets (i.e., a limited number of interferograms) and on their low temporal variability.

The multi-look and single-look phase target candidates are then combined in a single vector list that is used in the decomposition of the interferometric phase, which is carried out through an iterative regression analysis, initialized using precise orbital ephemeris and the Shuttle Radar Topography Mission (SRTM) 1 arc-second Digital Elevation Model (DEM) [32] of the test area.

At the beginning, the phase model focuses solely on estimating relative terrain height corrections between point target pairs, assuming negligible time-dependent deformation due to the short temporal separation between interferograms. However, in early iterations, the phase noise remains significant due to unmodeled atmospheric turbulence and residual orbital phase trends, especially affecting target pairs with substantial spatial separation.

To mitigate this, the algorithm is adapted to utilize multiple spatial patches, each containing a locally defined reference point. Regression is then performed between nearby patches, minimizing the distance between targets and thereby reducing noise. The resulting phase residuals are interpreted as the atmospheric phase screen (APS), including both height-dependent and turbulent delay components.

Phase unwrapping is performed in map geometry coordinates to minimize foreshortening and layover distortions, which are prevalent in mountainous regions. This significantly reduces processing errors and decreases the number of discarded targets [33]. The removal of these geometric distortions enables the inclusion of a greater number of measuring points (MPs) with higher temporal coherence.

These phase components are subsequently removed from the differential phase, and a new regression iteration is performed. After each iteration, improved estimates of the APS, corrections to DEM-derived heights, and masks for discarding decorrelated targets are produced. The process is repeated until the model stabilizes and the interferometric phase noise is sufficiently reduced, allowing for regression within a single patch. This final single-patch regression is two-dimensional, considering both the linear dependence of topographic phase on the perpendicular baseline and the temporal evolution of deformation.

Despite the benefits of multi-looking, residual noise may persist due to non-zero closure phases, which cannot be fully corrected through additional spatial filtering [34,35] limiting the reliability of phase interpretation.

The second stage addresses this by focusing exclusively on single-look phases, leveraging the atmospheric and topographic corrections derived in the first step. Notably, the Sentinel-1 mission's orbit stability, maintaining a 200 m Earth-fixed tube, relaxes the spatial constraints typically required for interferometric suitability. This reduces the distinction between point-like targets (PS) and distributed scatterers (DS). Moreover, using image stacks spanning six months facilitates the identification of DS targets with high temporal coherence (e.g., gravel surfaces, sparsely vegetated regions) alongside PS targets (e.g., buildings, exposed bedrock) [31]. This enables the inclusion of single-look distributed targets in the regression analysis, which is iteratively refined until a consistent phase model is achieved and reliable phase unwrapping is ensured.

Finally, the multi-reference unwrapped phases are resolved using a Singular Value Decomposition (SVD) approach, which provides a least-squares solution for estimating the phase deformation time series.

Overall, HIA is a customized approach designed to enhance the EGMS's landslide HIA all detection capability by integrating multiple A-DInSAR techniques and algorithms. It leverages selected point-like phase targets and optimizes spatial and temporal relationships among radar acquisitions, fully exploiting the orbit stability and short revisit time of the Sentinel-1 mission to produce an unconventional interferometric time series, considerably shorter than those generated by standard TS-InSAR methods.

The EGMS products are generated by a consortium of four distinct InSAR Processing Entities (IPEs). As a result, variations exist among the processing algorithms used in their respective processing chains. Nevertheless, the final products share the same attributes and collectively meet the project's standards for quality, consistency, and homogeneity. The main characteristics of the four IPEs are summarized in Table 2.

Table 2. Main characteristics of the IPE.

IPE	E-Geos	TRE ALTAMIRA	NORCE	GAF/DLR
Algorithm Name	PSP-IFSAR	SqueeSAR	GSAR-GTSI	PSI
Selection of MP candidates	Persistent Scatterer Pair (PSP)	Amplitude Dispersion Index (PS) + Coherence analysis (DS)	Thresholding achieved RMS deviation from a fitted polynomial + seasonal model	SCR (Signal-to-Clutter Ratio) and ADI (Amplitude Dispersion Index)
Phase Unwrapping	Sparse Multidimensional Domain	Lp-norm inversion of the connectivity matrix describing pixels pairs	L1-norm inversion of the identified spatial primary network	LAMBDA estimator + L1 outlier rejection + L2 inversion for integration of the signal model parameters
Atmospheric Estimation	Inverse distance weighting for turbulent components	Low pass filter	Kriging of the phase residuals of the identified primary network	Adaptive from an estimate of the atmospheric variogram

A detailed and comprehensive description of the EGMS processing strategy, which was beyond the scope of this paper, is provided in [36].

EGMS products comprise a continuously updated 5-year rolling dataset, with annual updates released separately since 2015. As of now, users can access time series data for

measurement points up to 2023, corresponding to the third update. In this study, we utilized the Basic (L2a) products, which include InSAR measurements of ground displacement along the sensor's line-of-sight (LOS) in both ascending and descending acquisition geometries. Similar to other geodetic methods, such as levelling and GNSS relative positioning, InSAR measurements are referenced to a specific point in space and a specific point in time. The Basic products are generated through the independent processing of individual SAR stacks using local reference points. These products are particularly suitable for monitoring and interpreting localized ground movements, such as landslides [18].

4. Results

Based on the Sentinel-1 mission's wavelength and revisit frequency, the theoretical maximum detectable differential LOS displacement rate between two radar scatterers exceeds 0.85 m/year [37]. This estimation assumes a 6-day revisit interval, made possible by the combined use of Sentinel-1A and Sentinel-1B data. However, the actual accuracy in estimating deformation rates is influenced by the signal-to-noise ratio and the specific phase unwrapping techniques applied to resolve phase ambiguities. It is important to highlight that this theoretical threshold refers to differential phases, i.e., those computed between pairs of radar scatterers. The effective ability to detect deformation at a specific target depends on the spatial characteristics of the deformation phenomenon (smoother deformations yield better results) and on the density of MPs within the affected area (higher densities provide more reliable measurements).

The HIA methodology is primarily designed to address and optimize these latter factors, incrementing the number of radar targets that could remain coherent under fast and non-uniform displacements, providing a spatial coverage sufficient to detect, map, and measure ground displacement caused by the largest possible variety of landslides. The HIA relies on the derivation of reliably unwrapped phases for the differential interferogram pairs of the multi-reference stack and the consequent interpretation of the phases with respect to parameters such as the topographic height correction, line-of-sight displacement, and atmospheric path delay.

Figure 3 presents the results obtained through HIA processing over the Cherz Plateau using the ascending dataset while Figure 4 shows the descending acquisitions. Figures 5 and 6 refer to the Corvara landslide.

Figures 7 and 8 present a side-by-side comparison between the EGMS Basic products, derived from both ascending and descending datasets, and the results of the five years of HIA processing superimposed in a single image, respectively, over the Cherz Plateau and the Corvara landslide. Since each HIA processing captures a different number and distribution (i.e., location) of scatterers, combining the five radar target sets into a single image enhances spatial sampling, thereby improving the detection of active landslides.

The displacement maps provide a clear qualitative comparison between the two approaches. Notably, the number of scatterers (i.e., measurement points) identified by the HIA was significantly higher than those detected by EGMS, resulting in denser spatial coverage for each year in the dataset. This improved density facilitates the easier identification of landslides on the map and their kinematic patterns; landslides on the Cherz Plateau and the Corvara in Badia mass movement are clearly visible in both the ascending and descending datasets. The observed shift in the LOS displacement between the ascending and descending acquisitions—evident from the color variations indicating motion toward and away from the satellite—suggests a predominant planar downslope component of movement. Both the direction and magnitude of this displacement are consistent with values reported in previous studies [25,28,30].

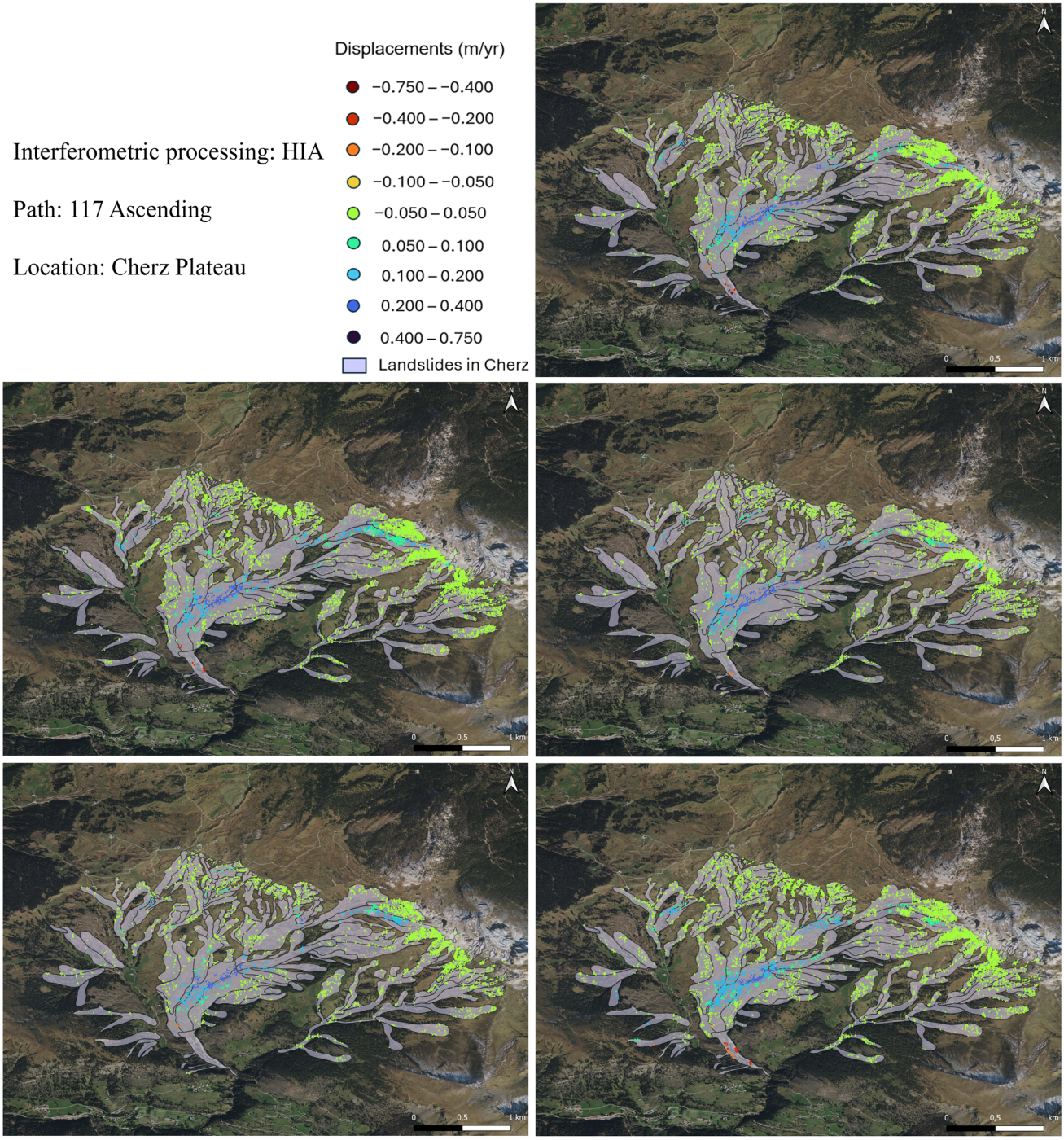


Figure 3. HIA results of the ascending dataset over the Cherz Plateau, shown in light purple, from 2017 to 2021 overlaid on an optical satellite image (Map data ©2022 Bing Satellite).

HIA allowed tracking of the displacement rates closest to the theoretical maximum detectable. Conversely, some slowly deforming slopes captured by EGMS appeared stable in the HIA results. This discrepancy arises because, over a short observation window (e.g., six months), it is not possible to effectively model APS effects. These can introduce phase errors exceeding 7.5 radians per year (equivalent to displacements of approximately 0.03 m/year), causing slowly moving areas to be mistaken for noise. To address this, the color scale was adjusted below this deformation threshold to reduce noise interpretation errors while still clearly highlighting areas of rapid displacement. It should therefore be emphasized that the figures use different LOS deformation scales for the EGMS and HIA datasets.

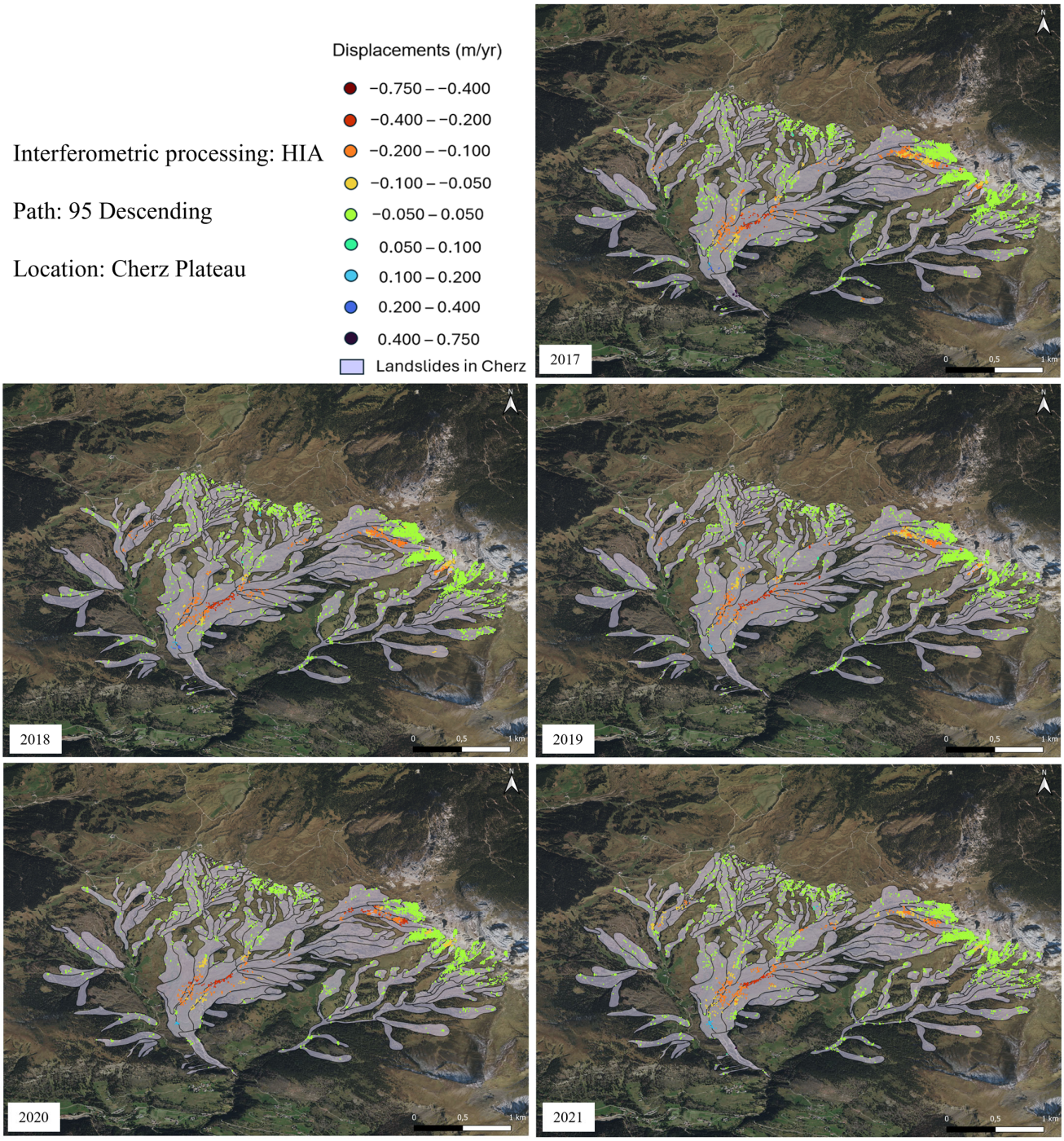


Figure 4. HIA results of the descending dataset over the Cherz Plateau, shown in light purple, from 2017 to 2021 overlaid on an optical satellite image (Map data ©2022 Bing Satellite).

When extending the analysis to the entire study area, the significantly denser spatial coverage of measurement points obtained through HIA processing became even more evident and noteworthy.

Overlaying the HIA displacement maps with the landslide contours from the IFFI project revealed numerous additional active landslides that were not detected by EGMS (Figures 9 and 10).

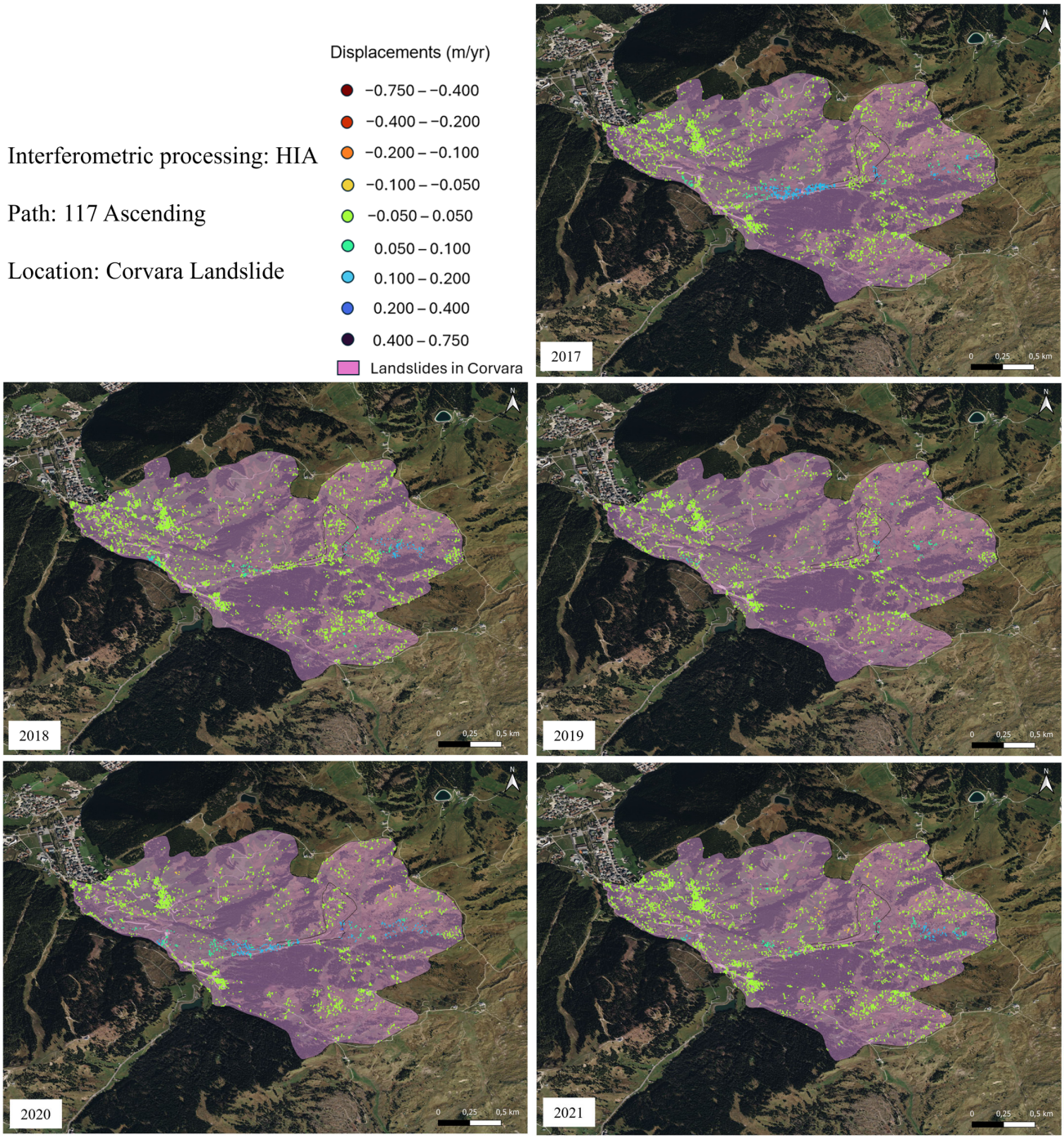


Figure 5. HIA results of the ascending dataset over the Corvara landslide, shown in fuchsia, from 2017 to 2021 overlaid on an optical satellite image (Map data ©2022 Bing Satellite).

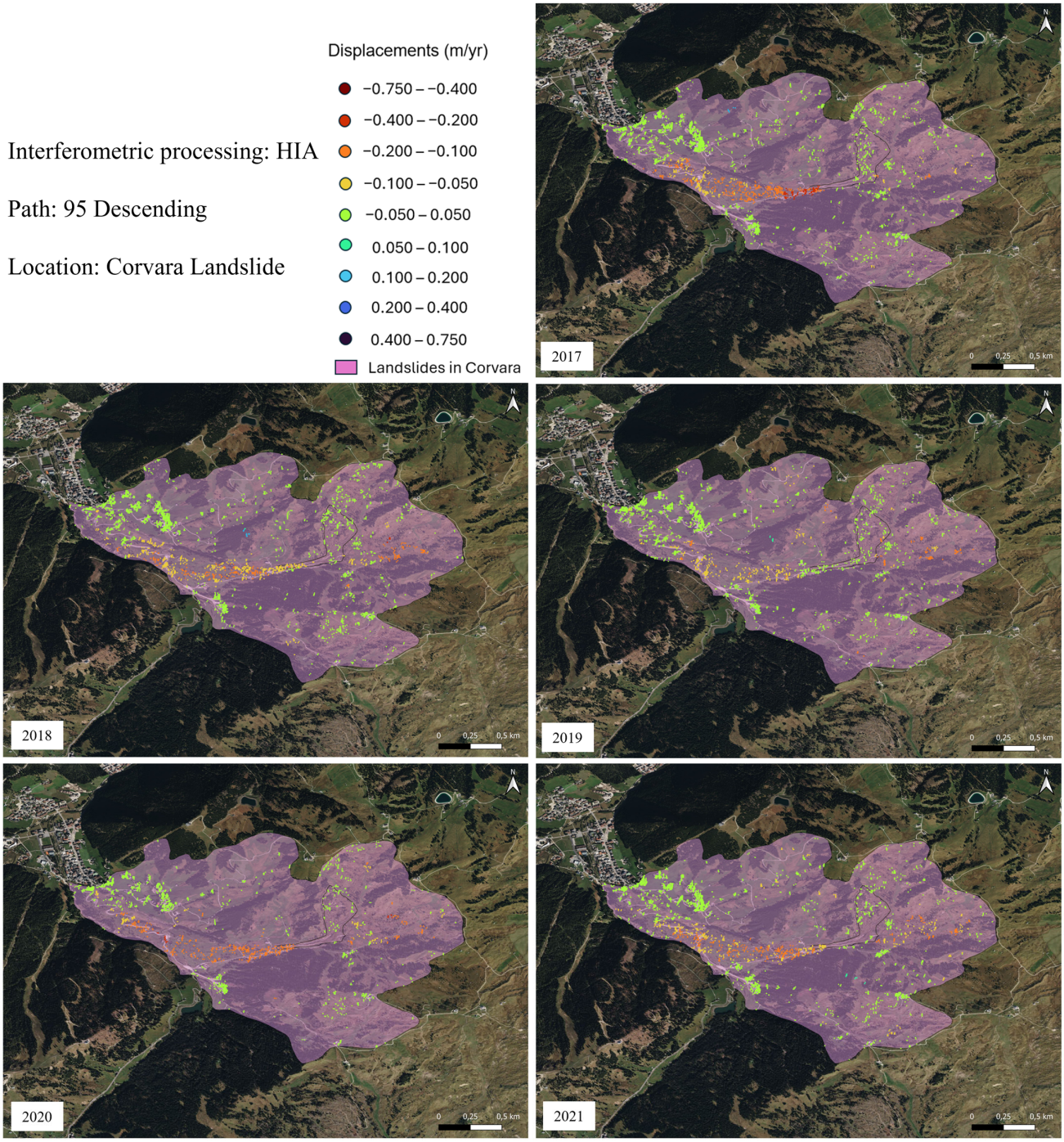


Figure 6. HIA results of the descending dataset over the Corvara landslide, shown in fuchsia, from 2017 to 2021 overlaid on an optical satellite image (Map data ©2022 Bing Satellite).

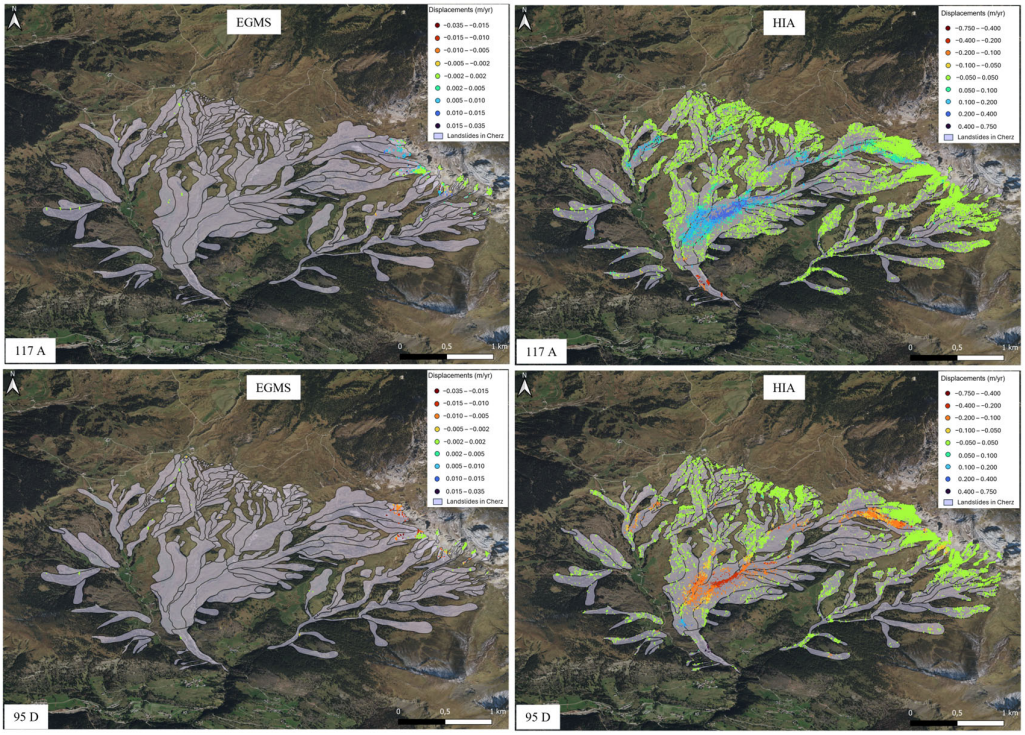


Figure 7. EGMS Basic products, derived from both the ascending (**top**) and descending datasets (**bottom**) over the Cherz Plateau, shown in light purple, compared to the results obtained through HIA processing from 2017 to 2021, superimposed on an optical satellite image (Map data ©2022 Bing Satellite). The color scale for the EGMS and the HIA is different.

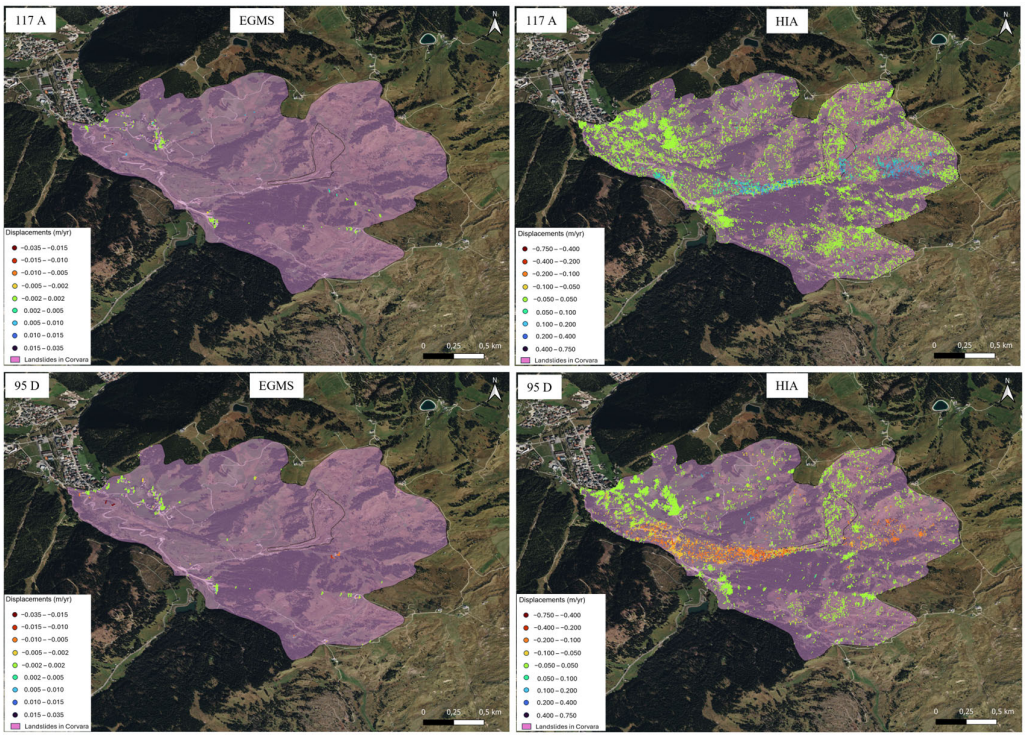


Figure 8. EGMS Basic products, derived from both the ascending and descending datasets over the Corvara landslide, shown in fuchsia, compared to the results obtained through HIA processing from 2017 to 2021 superimposed on an optical satellite image (Map data ©2022 Bing Satellite). The color scale for the EGMS and the HIA is different.

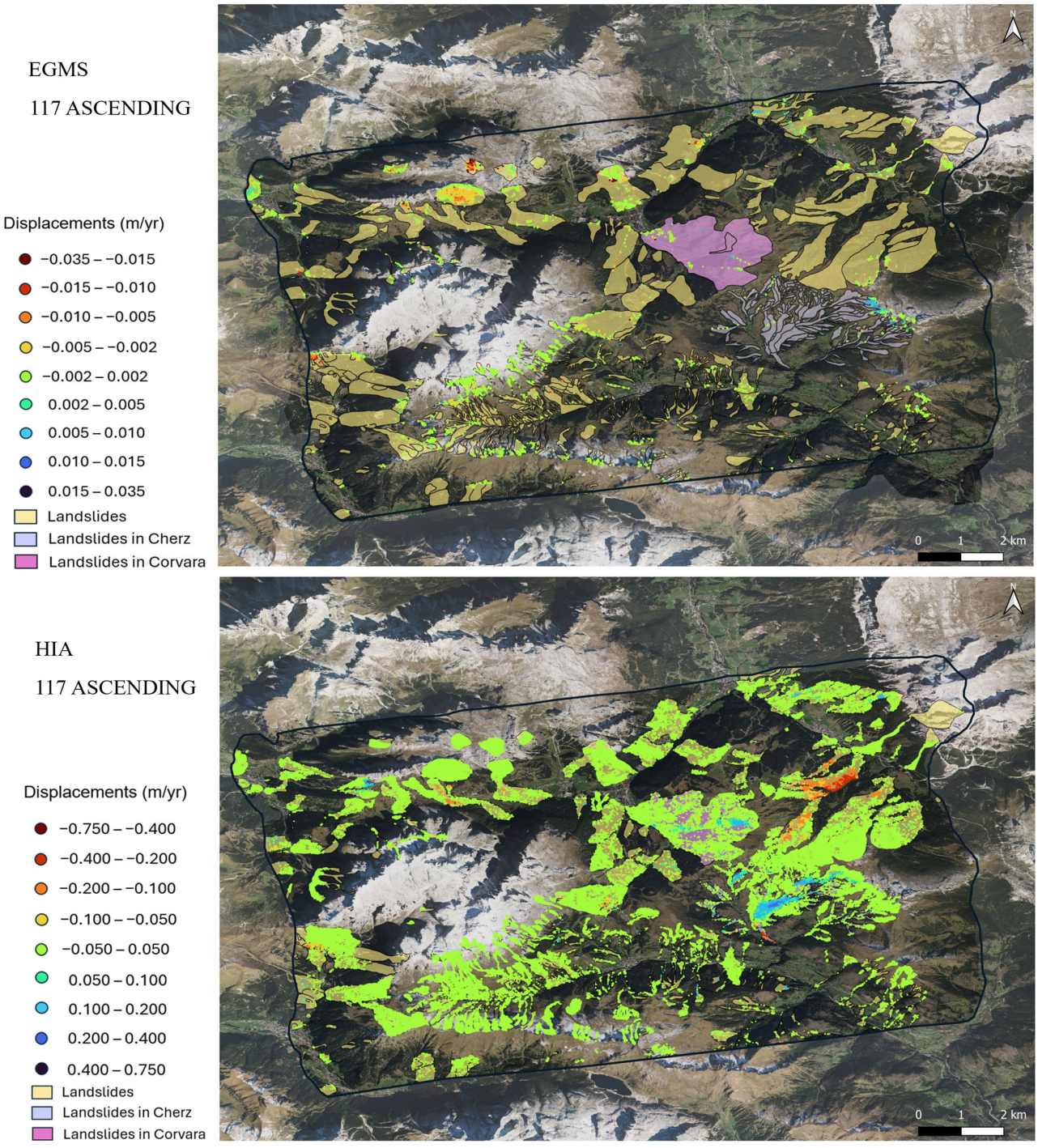


Figure 9. EGMS Basic products (2017–2021), derived from ascending dataset over the test site compared to the results obtained through HIA processing from 2017 to 2021 superimposed on an optical satellite image (Map data ©2022 Bing Satellite). Only radar targets located within the boundaries of the 910 landslides mapped in the Italian Landslide Inventory (IFFI Project) are shown. The Corvara landslides are shown in fuchsia, and the Cherz Plateau is shown in light purple. The color scale for the EGMS and the HIA is different.

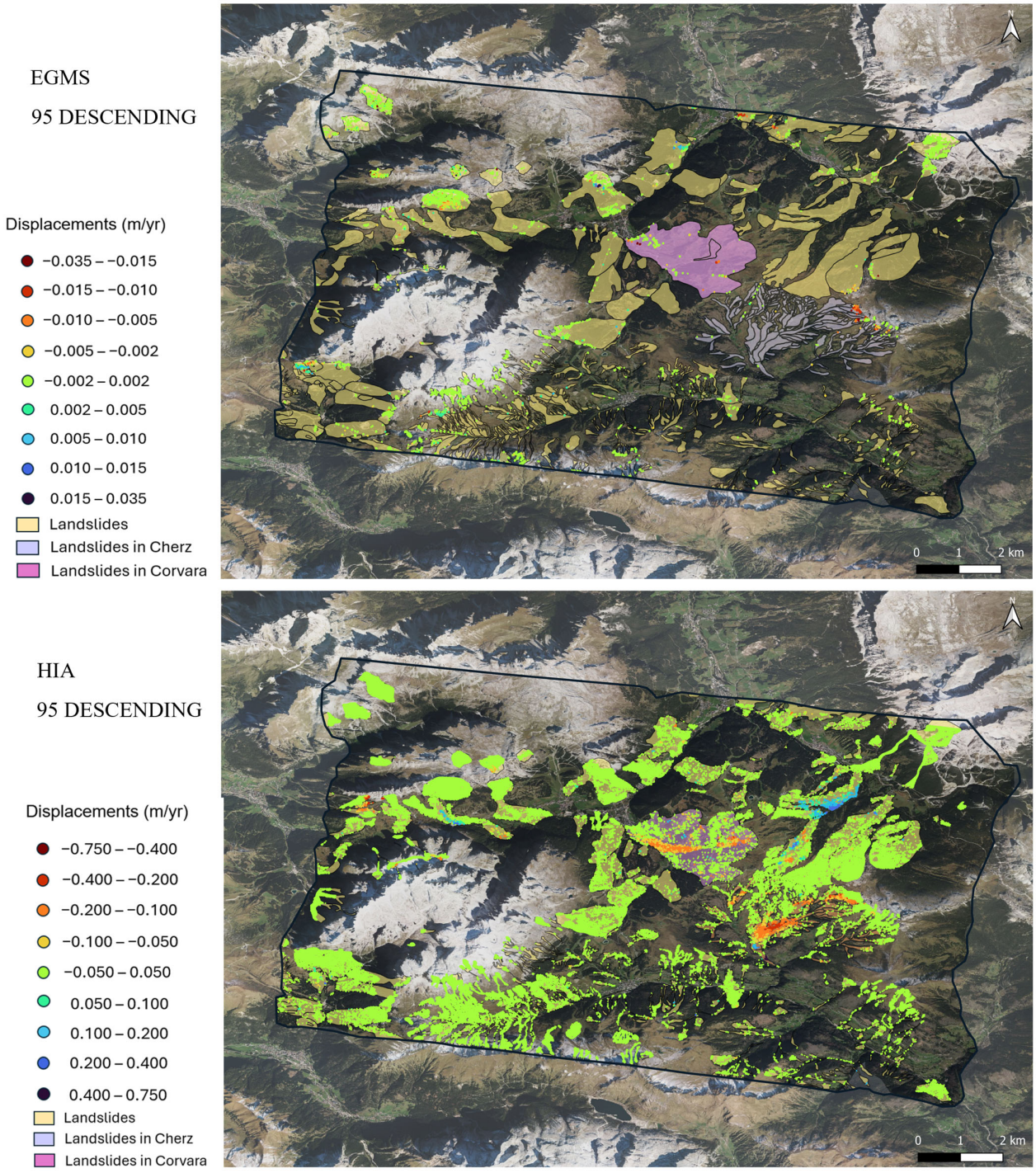


Figure 10. EGMS Basic products (2017–2021), derived from the descending dataset over the test site compared to the results obtained through HIA processing from 2017 to 2021 superimposed on an optical satellite image (Map data ©2022 Bing Satellite). Only radar targets located within the boundaries of the 910 landslides mapped in the Italian Landslide Inventory (IFFI Project) are shown. The Corvara landslides are shown in fuchsia, and the Cherz Plateau is shown in light purple. The color scale for the EGMS and the HIA is different.

5. Discussion

In the EGMS processing chain, all Sentinel-1 acquisitions are co-registered to a single primary reference image, carefully chosen to minimize the dispersion of temporal and geometrical baselines while maximizing the average coherence across the entire dataset.

In contrast, the HIA processing approach co-registers the acquisitions of each individual year to a different reference image selected within that same year, for the same purpose. Consequently, in a five-year time series, HIA employs five distinct reference images, causing slight variations in acquisition geometry over the same area. As a result, the MPs are not guaranteed to correspond exactly from year to year, since it is not possible to precisely define the scattering mechanism within the resolution cell.

On the one hand, this might prevent stacking the MPs across years and applying a linear regression-based approach to extend the time series to five years, as conducted in the EGMS processing over snow-covered regions. On the other hand, for detection purposes, this variability can actually enhance the capability to distinguish active landslide sectors by increasing the spatial distribution of MP, as illustrated in Figures 7–10.

Despite the inherent limitations, some HIA targets—due to their spatial proximity—can be considered nearly identical and thus comparable over time. Figures 11 and 12 show the five-year time series of two such points (one on the ascending acquisition and one on descending), each compared with a MP from the EGMS, for the Cherz and Corvara test sites, respectively.

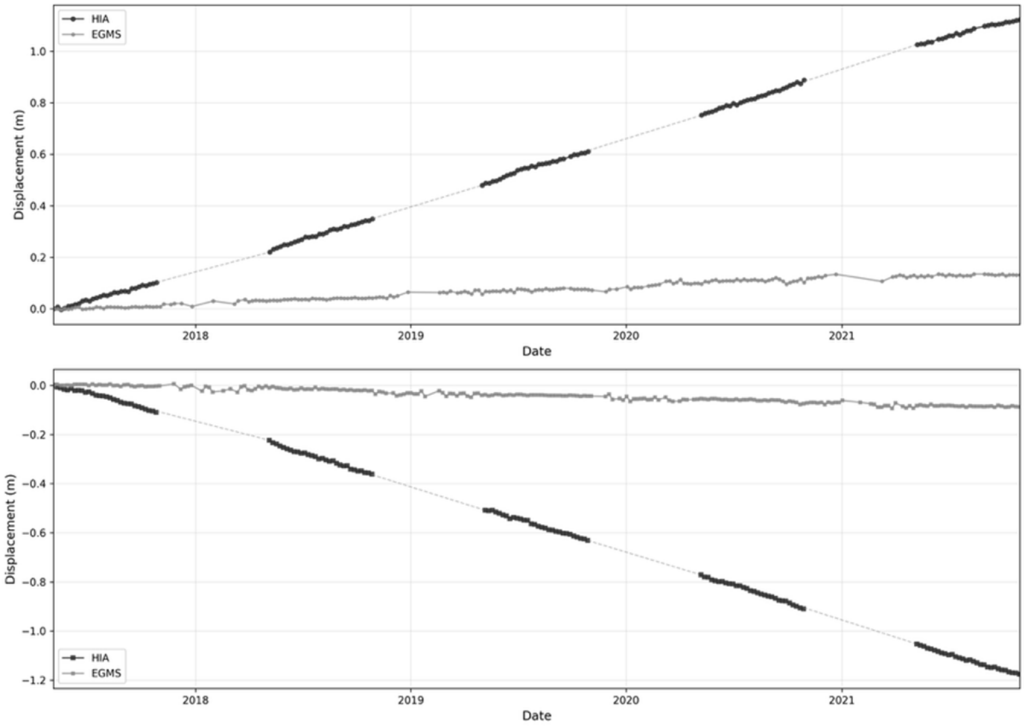


Figure 11. LOS displacement time series of two of the fastest MPs detected by HIA and EGMS over the Cherz Plateau. The **top** and **bottom** graphs correspond to the ascending and descending datasets, respectively. The series were extended to five years using a linear regression approach.

The comparison focused on radar targets exhibiting the highest displacement velocities in both HIA and EGMS. In other words, targets were selected based on maximum recorded displacements rather than spatial proximity, given the limited availability of EGMS MPs within the landslide areas.

This approach highlights the capability of HIA to detect faster-moving targets, as clearly illustrated in the figures. Assuming the validity of the linear regression-based method used to extend the HIA time series to five years, the accumulated LOS displacement for a sector of the landslide could reach up to almost 1.20 m.

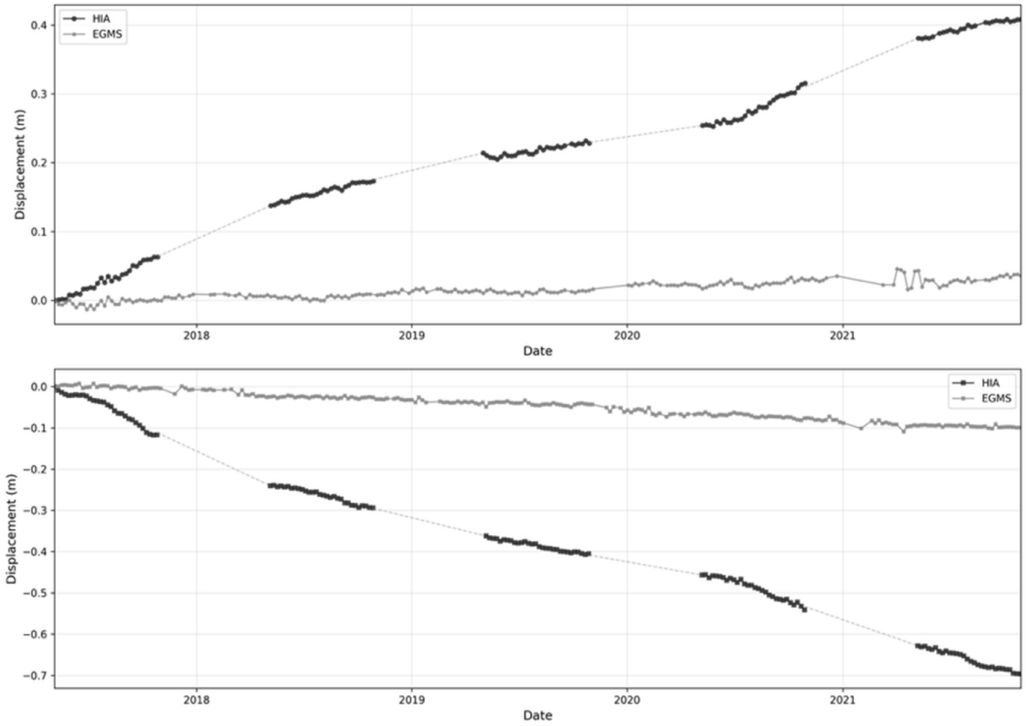


Figure 12. LOS displacement time series of two of the fastest MPs detected by HIA and EGMS over the Corvara landslide. The **top** and **bottom** graphs correspond to the ascending and descending datasets, respectively. The series were extended to five years using a linear regression approach.

For the Corvara dataset (Figure 12), a potentially nonlinear displacement behavior was also evident.

The EGMS framework is based on a wide-area processing (WAP) approach, enabling the analysis of extensive continental-scale regions. Operating on large and continuous datasets, EGMS applies atmospheric corrections using numerical meteorological models (ECMWF, ERA5) combined with statistical spatial discrimination techniques. Final calibrations are then performed to align the radar measurements with the three-dimensional geodetic reference frame, supported by a dedicated geodetic calibration infrastructure that relies on European GNSS networks.

HIA, in contrast, provides a faster and more detailed analysis focused on smaller areas and a reduced number of images. It is specifically designed to locally complement and refine EGMS products, which, due to their broad-scale nature, may not fully capture localized phenomena.

Both EGMS and HIA algorithms process full-resolution measurement points. However, while EGMS emphasizes the temporal stability of radar reflectors over long time spans—resulting in lower point densities but higher reliability for detecting millimeter- to sub-centimeter-scale displacements associated with slow, continuous deformations—HIA is optimized for detecting faster and potentially nonlinear deformations, reaching up to tens of centimeters per year. This increased sensitivity comes at the expense of detecting slower movements, which may be obscured by noise introduced by limited tropospheric delay compensation.

Figure 13 presents histograms that offer a quantitative comparison, highlighting the substantial difference in the number of MPs identified by EGMS and HIA over the Cherz and Corvara landslides, as well as across other mass movements within the study area.

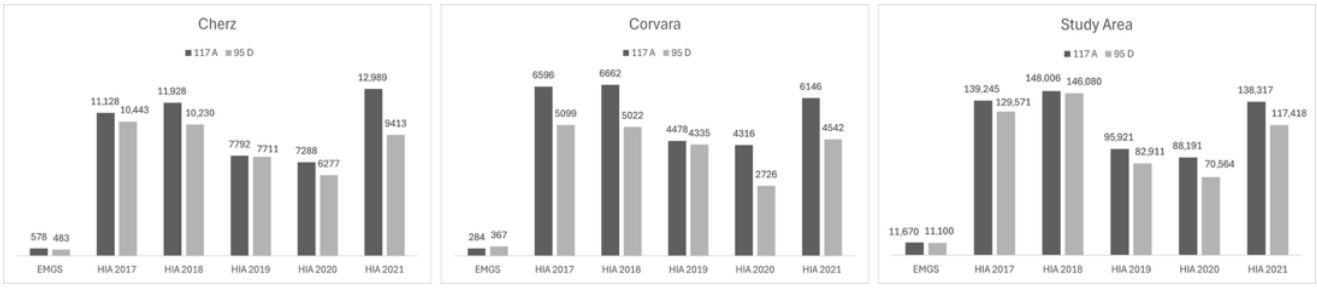


Figure 13. Histograms showing the number of radar targets detected by EGMS and yearly HIA processing for the Cherz landslide (**left**), the Corvara landslide (**middle**), and for all mapped mass movements within the study area (**right**).

The variability in the number of radar targets detected using the HIA processing is evident in both the ascending and descending datasets. This variation appears to be primarily influenced by weather conditions (e.g., snow cover) rather than differences in processing procedures (see Table 1), highlighting the robustness of the HIA methodology even in the presence of missing acquisitions. Another key takeaway from the histograms is that, even in 2020—the year with the lowest number of detected radar targets—HIA still identified more than six times the number of scatterers to EGMS. On average, across the study area, HIA detected approximately ten times more measurement points than EGMS over the landslide bodies (Figure 14).

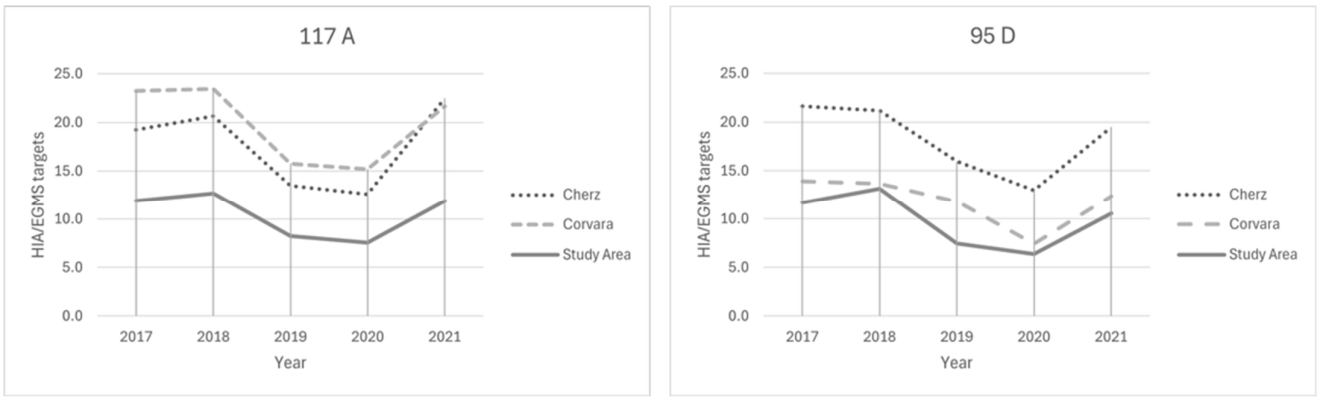


Figure 14. Yearly variation in the ratio of radar targets detected by HIA compared to EGMS, shown for the ascending dataset (**left**) and the descending dataset (**right**).

Finally, by defining a landslide as active when it contains at least ten radar targets showing significant displacement rates (i.e., exceeding ± 0.002 m/year for EGMS products and ± 0.050 m/year for HIA results), the HIA processing identified over three times more active landslides than the EGMS products. In other words, within the study area, HIA detected more than three times as many active landslides as EGMS.

In addition to the direct comparison with EGMS products, the HIA results showed strong consistency with the landslides mapped in the Italian Landslide Inventory (IFFI Project). For the specific cases of the Cherz and Corvara sites, the findings are further corroborated by six independent bibliographic references (see Section 2), which confirm both the presence and kinematic behavior of the mapped landslides.

6. Conclusions

Any method or technique that leverages SAR interferometry to monitor the displacement of coherent targets relies on measuring distances using electromagnetic waves. As such, it is inherently influenced by the wavelength and revisit time (that dictates the tempo-

ral sampling), technical parameters that vary across space missions and cannot be adjusted by the user.

Space-borne SAR interferometry enables the detection and monitoring of landslide-induced displacements, provided the following conditions are met:

- The landslide is active during the observation period.
- The displacement rate and direction align with the technical parameters of the satellite mission.

In other words, a landslide can only be detected if its LOS displacement component is measurable within the constraints imposed by the specific mission. This holds true regardless of landslide type and processes, including the material and the state, distribution, style of activity [38]. Moreover, detection depends on the availability of radar targets that remain coherent throughout the observation period, conditions typically favored in areas with sparse or no vegetation. Thus, landslides occurring above the tree line (the edge of a habitat at which trees are capable of growing) are more likely to be detected.

Despite these limitations, SAR interferometric processing can be optimized to detect a broader range of landslides than is currently possible with the EGMS.

The proposed methodology is tailored to identify landslides, with displacement rates on the order of tens of centimeters per year, an order of magnitude higher than those typically detected by EGMS.

The approach prioritizes the detection of faster-moving landslides by maximizing the number of coherent targets, albeit at the cost of reduced sensitivity to slower-moving events. By broadening the spectrum of detectable landslides, this method complements and strengthens existing EGMS products and contributes valuable insights to landslide risk assessment and mitigation efforts through improved coverage of critical ground measurement points.

Moreover, its applicability could extend beyond mountainous areas to regions with sparse vegetation, enabling the analysis of any ground deformation induced hazard driven by natural or anthropogenic factors.

Overall, HIA's improved ability to detect ground deformation enhances the effectiveness of A-DInSAR techniques in identifying, mapping, and monitoring natural hazards, thereby providing vital support for sustainable land management, infrastructure protection, and climate change adaptation.

Author Contributions: M.M.: conceptualization, methodology, supervision, project administration, writing—original draft. F.C.: methodology, visualization, writing—original draft. A.B.: software, investigation, writing—reviewing and editing. E.B.: software, validation, formal analysis, writing—reviewing and editing. G.B.: resources, writing—reviewing and editing. G.M.: data curation, writing—reviewing and editing. A.P.: funding acquisition, writing—reviewing and editing. All authors have read and agreed to the published version of the manuscript.

Funding: This research was carried out within the framework of the VAIALAND Project and joint research agreement funded by the Veneto Region (Italy).

Data Availability Statement: The raw data supporting the conclusions of this article will be made available by the authors on request.

Acknowledgments: The authors acknowledge the European Space Agency for providing the Sentinel-1 radar images. SAR interferometric analyses were performed using Gamma Remote Sensing AG (Gümligen, Switzerland). Figures and graphs were produced with QGIS version 3.40 LTR Bratislava and GMT version 3.1.

Conflicts of Interest: The authors declare no conflicts of interest.

Abbreviations

The following abbreviations are used in this manuscript:

SAR	Synthetic Aperture Radar
A-DInSAR	Advanced Differential Interferometry SAR
TS-InSAR	Time Series Interferometric SAR
PSI	Persistent Scatterers Interferometry
SBAS	Small Baseline Subsets
InSAR	Interferometric Synthetic Aperture Radar
EU	European Union
EGMS	European Ground Motion Service
PS	Persistent Scatterers
DS	Distributed Scatterers
GNSS	Global Navigation Satellite System
HIA	Hybrid Interferometric Approach
UNESCO	United Nations Educational, Scientific and Cultural Organization
IFFI	Inventario dei Fenomeni Franosi in Italia
ISPRA	Istituto Superiore per la Protezione e la Ricerca Ambientale
TDR	Time Domain Reflectometry
SRTM	Shuttle Radar Topography Mission
DEM	Digital Elevation Model
APS	Atmospheric Phase Screen
MP	Measuring Points
SVD	Singular Value Decomposition
IPE	InSAR Processing Entities
LOS	Line Of Sight
WAP	Wide Area Processing
ECMWF	European Centre for Medium-Range Weather Forecasts
ERA5	Re-Analysis of ECMWF version 5

References

1. Massonnet, D.; Rossi, M.; Carmona, C.; Ardagna, F.; Peltzer, G.; Feigl, K.; Rabaoute, T. The displacement field of the Landers earthquake mapped by radar interferometry. *Nature* **1993**, *364*, 138–142. [CrossRef]
2. Massonnet, D.; Feigl, K.L. Radar interferometry and its application to changes in the Earth's surface. *Rev. Geophys.* **1998**, *36*, 441–500. [CrossRef]
3. Rosen, P.A.; Hensley, S.; Joughin, I.R.; Li, F.K.; Madsen, S.N.; Rodriguez, E.; Goldstein, R.M. Synthetic aperture radar interferometry. *Proc. IEEE* **2000**, *88*, 333–382. [CrossRef]
4. Caltagirone, F.; Spera, P.; Vigliotti, R.; Manoni, G. SkyMed/COSMO mission overview. In Proceedings of the IGARSS '98. Sensing and Managing the Environment. 1998 IEEE International Geoscience and Remote Sensing. Symposium Proceedings, Seattle, WA, USA, 6–10 July 1998; Volume 2, pp. 683–685.
5. González Bonilla, M.J.; Cuerda Muñoz, J.M.; Casal Vázquez, N.; Hiedra Priego, C. The Scientific Exploitation of PAZ mission: PAZ Ciencia objectives and status. *Procedia Comput. Sci.* **2024**, *239*, 2223–2227. [CrossRef]
6. Ohki, M.; Motohka, T.; Kankaku, Y.; Miura, S.H.; Tadono, T.; Arikawa, Y. Advanced Land Observing Satellite-4: Mission Concepts and Technical Overview: Pioneering a new era of L-band SAR. *IEEE Geosci. Remote Sens. Mag.* **2025**, *13*, 35–40. [CrossRef]
7. Palomeque, M.; Ferreyra, J.; Thibeault, M. Monitoring Results of the SAOCOM-1 Constellation: A mission overview and summary of results. *IEEE Geosci. Remote Sens. Mag.* **2025**, *13*, 49–57. [CrossRef]
8. Quiroz, A.E.N.; Bartusch, M.; Stettner, S.; Moreira, A.; Zink, M. An Overview of the German Spaceborne X-Band SAR Program. In Proceedings of the IGARSS '22. IEEE International Geoscience and Remote Sensing Symposium, Kuala Lumpur, Malaysia, 17–22 July 2022; pp. 5436–5439.
9. Rosen, P.A.; Bawden, G.W.; Barela, P.; Chapman, B.; Fattahi, H.; Jones, C.E.; Joughin, I.R.; Lavalle, M.; Lohman, R.B.; Simons, M.; et al. The NASA-ISRO SAR Mission: A summary. *IEEE Geosci. Remote Sens. Mag.* **2025**, *13*, 8–34. [CrossRef]
10. Thompson, A.A. Overview of the RADARSAT Constellation Mission. *Can. J. Remote Sens.* **2015**, *41*, 401–407. [CrossRef]
11. Torres, R.; Snoeij, P.; Geudtner, D.; Bibby, D.; Davidson, M.; Attema, E.; Potin, P.; Rommen, B.; Floury, N.; Brown, M.; et al. GMES Sentinel-1 mission. *Remote Sens. Environ.* **2012**, *120*, 9–24. [CrossRef]

12. Hooper, A. A multi-temporal InSAR method incorporating both persistent scatterer and small baseline approaches. *Geophys. Res. Lett.* **2008**, *35*, 16. [CrossRef]
13. Ferretti, A.; Fumagalli, A.; Novali, F.; Prati, C.; Rocca, F.; Rucci, A. A New Algorithm for Processing Interferometric Data-Stacks: SqueeSAR. IEEE Trans. *Geosci. Remote Sens.* **2011**, *49*, 3460–3470. [CrossRef]
14. Werner, C.; Wegmuller, U.; Strozzi, T.; Wiesmann, A. Interferometric point target analysis for deformation mapping. In Proceedings of the 2003 IEEE International Geoscience and Remote Sensing Symposium, Toulouse, France, 21–25 July 2003; Volume 7, pp. 4362–4364.
15. Ferretti, A.; Prati, C.; Rocca, F. Permanent scatterers in SAR interferometry. *IEEE Trans. Geosci. Remote Sens.* **2001**, *39*, 8–20. [CrossRef]
16. Berardino, P.; Fornaro, G.; Lanari, R.; Sansosti, E. A new algorithm for surface deformation monitoring based on small baseline differential SAR interferograms. *IEEE Trans. Geosci. Remote Sens.* **2002**, *40*, 2375–2383. [CrossRef]
17. Solari, L.; Lege, T.; Kalia, A.; Lanari, R.; Hooper, A. Wide area ground motion data: Lessons learnt and future perspectives. EUSAR 2024. In Proceedings of the 15th European Conference on Synthetic Aperture Radar, Munich, Germany, 23–26 April 2004; pp. 104–109.
18. Costantini, M.; Minati, F.; Trillo, F.; Ferretti, A.; Novali, F.; Passera, E.; Dehls, J.; Larsen, Y.; Marinkovic, P.; Eineder, M.; et al. European Ground Motion Service (EGMS). In Proceedings of the IEEE International Geoscience and Remote Sensing Symposium IGARSS, Brussels, Belgium, 11–16 July 2001; pp. 3293–3296.
19. Guzzetti, F. Invited perspectives: Landslide populations—Can they be predicted? *Nat. Hazards Earth Syst. Sci.* **2021**, *21*, 1467–1471. [CrossRef]
20. Van Den Eeckhaut, M.; Hervás, J. *Landslide Inventories in Europe and Policy Recommendations for Their Interoperability and Harmonisation—A JRC Contribution to the EU-FP7 SafeLand Project*; JRC Report EU 25666 EN; Publications Office of the European Union: Luxembourg, 2021.
21. Solari, L.; Del Soldato, M.; Raspini, F.; Barra, A.; Bianchini, S.; Confuorto, P.; Casagli, N.; Crosetto, M. Review of Satellite Interferometry for Landslide Detection in Italy. *Remote Sens.* **2020**, *12*, 1351. [CrossRef]
22. Colesanti, C.; Wasowski, J. Investigating landslides with space-borne Synthetic Aperture Radar (SAR) interferometry. *Eng. Geol.* **2006**, *88*, 173–199. [CrossRef]
23. ISPRA. Regioni. Progetto IFFI—Inventario dei Fenomeni Franosi in Italia. Istituto Superiore per la Protezione e la Ricerca Ambientale. Available online: https://www.progettoiffi.isprambiente.it (accessed on 6 May 2025).
24. Panizza, M.; Corsini, A.; Ghinoi, A.; Marchetti, M.; Pasuto, A.; Soldati, M. Explanatory notes of the geomorphological map of the Alta Badia Valley (Dolomites, Italy). *Geogr. Fis. Din. Quat.* **2011**, *34*, 105–126.
25. Tagliavini, F.; Mantovani, M.; Marcato, G.; Pasuto, A.; Silvano, S. Validation of landslide hazard assessment by means of GPS monitoring technique—A case study in the Dolomites (Eastern Alps, Italy). *Nat. Hazards Earth Syst. Sci.* **2007**, *7*, 185–193. [CrossRef]
26. Corsini, A.; Pasuto, A.; Soldati, M. Geomorphological investigation and management of the Corvara landslide (Dolomites, Italy). *Trans. Jpn. Geomorphol. Union* **1999**, *20*, 169–186.
27. Corsini, A.; Pasuto, A.; Soldati, M.; Zannoni, A. Field monitoring of the Corvara landslide (Dolomites, Italy) and its relevance for hazard assessment. *Geomorphology* **2005**, *66*, 149–165. [CrossRef]
28. Schlögel, R.; Thiebes, B.; Mulas, M.; Cuozzo, G.; Notarnicola, C.; Schneiderbauer, S.; Crespi, M.; Mazzoni, A.; Mair, V.; Corsini, A. Multi-Temporal X-Band Radar Interferometry Using Corner Reflectors: Application and Validation at the Corvara Landslide (Dolomites, Italy). *Remote Sens.* **2017**, *9*, 739. [CrossRef]
29. Mulas, M.; Petitta, M.; Corsini, A.; Schneiderbauer, S.; Mair, F.V.; Iasio, C. Long-term monitoring of a deep-seated, slow-moving landslide by mean of C-band and X-band advanced interferometric products: The Corvara in Badia case study (Dolomites, Italy). *Int. Arch. Photogramm. Remote Sens. Spat. Inf. Sci.* **2015**, *XL-7/W3*, 827–829. [CrossRef]
30. Darvishi, M.; Schlögel, R.; Kofler, C.; Cuozzo, G.; Rutzinger, M.; Zieher, T.; Toschi, I.; Remondino, F.; Mejia-Aguilar, A.; Thiebes, B.; et al. Sentinel-1 and Ground-Based Sensors for Continuous Monitoring of the Corvara Landslide (South Tyrol; Italy). *Remote Sens.* **2018**, *10*, 1781. [CrossRef]
31. Wegmüller, U.; Magnard, C.; Werner, C.; Strozzi, T.; Caduff, R.; Manconi, A. Methods to avoid being affected by non-zero closure phase in InSAR time series analysis in a multi-reference stack. *Procedia Comput. Sci.* **2021**, *181*, 511–518. [CrossRef]
32. Rabus, B.; Eineder, M.; Roth, A.; Bamler, R. The shuttle radar topography mission—A new class of digital elevation models acquired by spaceborne radar. *ISPRS J. Photogramm. Remote Sens.* **2003**, *57*, 241–262. [CrossRef]
33. Magnard, C.; Wegmüller, U.; Werner, C. Persistent Scatterer Interferometry in mountainous areas: Advantages of working in map geometry. *Procedia Comput. Sci.* **2021**, *181*, 198–205. [CrossRef]
34. De Zan, F.; Zonno, M.; Lopez-Dekker, P. Phase Inconsistencies and Multiple Scattering in SAR Interferometry. *IEEE Trans. Geosci. Remote Sens.* **2015**, *53*, 6608–6616. [CrossRef]

35. Zwieback, S.; Liu, X.; Antonova, S.; Heim, B.; Bartsch, A.; Boike, J.; Hajnsek, I. A Statistical Test of Phase Closure to Detect Influences on DInSAR Deformation Estimates Besides Displacements and Decorrelation Noise: Two Case Studies in High-Latitude Regions. *IEEE Trans. Geosci. Remote Sens.* **2016**, *54*, 5588–5601. [CrossRef]
36. Ferretti, A.; Passera, E.; Capes, R. End-to-End Implementation and Operation of the European Ground Motion Service (EGMS). Algorithm Theoretical Basis Document. EGMS-SC1. Available online: https://land.copernicus.eu/user-corner/technical-library/egms-algorithm-theoretical-basis-document (accessed on 7 November 2025).
37. Crosetto, M.; Monserrat, O.; Cuevas-González, M.; Devanthéry, N.; Crippa, B. Persistent Scatterer Interferometry: A review. *ISPRS J. Photogramm. Remote Sens.* **2016**, *115*, 78–89. [CrossRef]
38. Cruden, D.M.; Varnes, D.J. Landslide Types and Processes. In *Landslides: Investigation and Mitigation*; Turner, A.K., Schuster, R.L., Eds.; National Academy of Sciences, The Transportation Research Board: Washington, DC, USA, 1996; Volume 247, pp. 36–75.

Disclaimer/Publisher's Note: The statements, opinions and data contained in all publications are solely those of the individual author(s) and contributor(s) and not of MDPI and/or the editor(s). MDPI and/or the editor(s) disclaim responsibility for any injury to people or property resulting from any ideas, methods, instructions or products referred to in the content.